Excitation mechanisms and gain modeling of the high-pressure atomic Ar laser in He/Ar mixtures

Jong W. Shon[a] and Mark J. Kushner[b]
University of Illinois, Department of Electrical and Computer Engineering, 1406 West Green Street, Urbana, Illinois 61801

(Received 22 September 1993; accepted for publication 3 November 1993)

The high-pressure (>0.5 atm) atomic Ar laser ($3d \rightarrow 4p$) oscillates on four infrared transitions (1.27–2.4 μm). Quasicontinuous oscillation on the 1.79 μm transition has been obtained using electron beam and fission-fragment excitation over a wide range of power deposition and gas pressure. In this regard, a computer model has been developed to investigate excitation mechanisms of the Ar laser. Results from the model suggest that the upper laser level of the 1.79 μm transition [$Ar(3d[1/2]_1)$] is dominantly populated by dissociative recombination of $HeAr^+$. In contrast, the dissociative recombination of Ar_2^+ is believed to predominantly produce $Ar(4s)$ states. Electroionization from Ar metastables at moderate to high pump rates is likely to be responsible for the high efficiency of the Ar laser. Gain and laser oscillation are discussed and compared to experiments for He/Ar gas mixtures using various Ar mole fractions and total pressures. These results show that the optimum Ar mole fractions in He/Ar mixtures are ~0.1%–5% for quasicontinuous pumping.

I. INTRODUCTION

The high-pressure (>0.5 atm) atomic Ar infrared laser operates on transitions between the $3d$ and $4p$ manifolds at wavelengths of 1.27 μm ($3d'[3/2]_1 \rightarrow 4p'\ [1/2]_1$), 1.69 μm ($3d[3/2]_0 \rightarrow 4p\ [3/2]_2$), 1.79 μm ($3d[1/2]_1 \rightarrow 4p\ [3/2]_2$), and 2.4 μm ($3d[1/2]_1 \rightarrow 4p'[1/2]_1$). (See Fig. 1.) The small amount of atmospheric absorption of the 1.27 and 1.79 μm transitions, the inherent long lifetime of rare gas mixtures, and the demonstrated high efficiency of the atomic Ar laser have renewed interest in optimizing its performance in large systems. For example, a parametric investigation of the fission-fragment excited Ar laser operating at 1.27 and 1.79 μm Ar transitions was recently reported by Hebner and Hays.[1,2] A peak power efficiency of 1.4% for the 1.79 μm transition at 760 Torr was obtained for He/Ar mixtures having Ar mole fractions of 0.3%–2.0%. An efficiency of 1.1% was reported for the 1.27 μm transition at 1300 Torr using a He/Ar=99.88/0.12 mixture.

Voinov *et al.*[3] have also recently reported on fission-fragment excitation of He/Ar and Ne/Ar mixtures in which they obtained lasing in Ar at 1.27, 1.69, and 1.79 μm. A maximum quasicontinuous output power of 390 W at 1.79 μm was obtained with an efficiency of 0.6% using a He/Ar=99.8/0.2 mixture at 2 atm. Mel'nikov and Sinyanskii[4] investigated the 1.149 μm transition ($4p[1/2]_1 - 4s'[1/2]_1$) in Ar using fission-fragment pumping and obtained a maximum laser power of 250 W with an efficiency of $\approx$0.1% (He/Ar=99.6/0.4 at 1520 Torr).

Similar laser performance has been demonstrated using electron beam excitation. Dudin *et al.*[5] reported lasing on three Ar transitions (1.27, 1.79, and 2.4 μm) with maximum gains of 0.028 cm^{-1} at 1.79 μm; and 0.021 cm^{-1} at 2.4 and 1.27 μm. The gas pressure was 2660 Torr and the gas mixture was He/Ar=99/1. Berkeliev *et al.*[6] have reported simultaneous lasing in Ar (1.79 μm) with a 2% efficiency and in N_2 (358 nm) with a 1% efficiency using a $He/Ar/N_2$=98.2/1.7/0.1 mixture at 2320 Torr.

The maximum theoretical intrinsic laser efficiency for the 1.79 μm transition with respect to the ground state is 2.3%. It is difficult to explain efficiencies of 1%–2% obtained in the cited experiments without there being an energy recirculation or electroionization process similar to the xenon laser.[7,8] Electroionization in rare gas lasers refers to recirculation of atomic states from the laser levels to the rare gas metastables followed by electron impact to the ion. Recombination of the ion then repopulates the upper laser level. This process is far more efficient than directly exciting the laser levels or creating ions from the ground state of the rare gas. In the context of this work we would like to generalize the term "electroionization" to include electron impact excitation of metastables to atomic levels higher than the upper laser levels as well as the ion.

To investigate the kinetics leading to high laser efficiency in the high-pressure Ar laser, we have developed and parametrized a computer model for the electron and fission-fragment excited laser. Results from the model and comparisons to experiments will be presented, and excitation mechanisms proposed for He/Ar mixtures. Our investigation suggests that dissociative recombination of $HeAr^+$ leads to excitation of the upper laser level in gas mixtures having moderate mole fractions of Ar (0.001–0.01). Self-quenching of the laser levels and population of $Ar(4s)$ by dissociative recombination of Ar_2^+ decreases laser power at higher Ar mole fractions.

The computer model and the proposed kinetics are described in Sec. II. A comparison of computed and experimental values of laser efficiency, small signal gain, and saturation flux are presented in Sec. III, followed by our concluding remarks in Sec. IV.

[a]Present address: Sandia National Laboratories, Dept. 8745, Livermore, CA 94551-0969.
[b]Author to whom correspondence should be addressed.

 0021-8979/94/75(4)/1883/8/$6.00 © 1994 American Institute of Physics

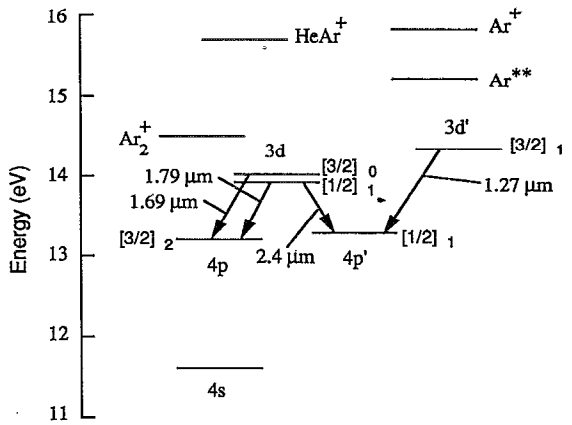

FIG. 1. Laser transitions and relevant atomic energy levels of Ar used in the model. The positions of $HeAr^+$ and Ar_2^+ are shown for reference. Laser oscillation at 1.79 μm occurs between $Ar(3d[1/2]_1)$ and $Ar(4p[3/2]_2)$.

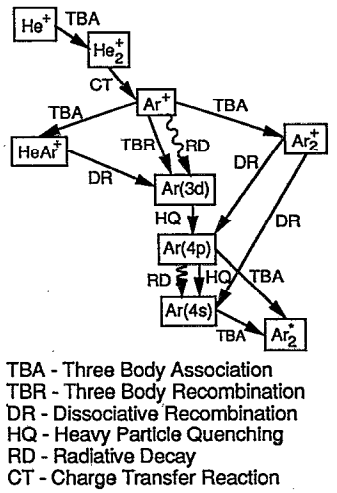

FIG. 2. Schematic of excitation and quenching pathways for the laser levels of the high-pressure atomic Ar laser. In our reaction scheme, excitation of the upper laser levels is dominated by dissociative recombination of $HeAr^+$. Quenching of the lower laser level is dominated by radiative relaxation and collisions with Ar.

II. DESCRIPTION OF THE MODEL

Our computer model is similar to models for particle beam excited excimer lasers,[9] and to our previously described models for atomic Xe and Ne lasers.[10,11] The model will therefore be only briefly described.

The model consists of a rate equation analysis of the time dependence of excitation and kinetics of particle beam excited He/Ar gas mixtures. There are 31 atomic and ion states included in the model for He, He^+, Ar, Ar^+, and their dimer ions (He_2^+, Ar_2^+, $HeAr^+$, $ArHe^+$). Of these species, eight atomic levels of Ar are included to resolve the three laser transitions at 1.27, 1.79, and 2.4 μm. The Ar levels used in the model are listed in Table I. Our reaction scheme differs from earlier models of the atomic Ar laser by Wilson *et al.*[12] and Basov *et al.*[13] by including more extensive plasma reaction chemistries and by resolving more transitions. A subset of the reactions included in the model are listed in Table II. A complete listing (286 processes) can be obtained by request from the authors.

The model begins by calculating W values (energy deposition/event) for ionization and excitation of all pertinent levels of each component of the gas mixture by the heavy ions. This calculation is performed with a Monte Carlo simulation (MCS) for the injected particles and secondary electrons for individual gas mixtures.[15] We relate W values obtained from an electron slowing calculation to those for heavy ions by using the scaling laws discussed in Ref. 27. The electron temperature is also obtained from the MCS. We parameterized the MCS to obtain a table of electron temperature as a function of excited state, electron densities, and gas mixture. This table was then interpolated during the actual kinetics calculation. The electron temperature and W values were then used to obtain rate coefficients, and rate equations for all species formulated. The rate equations were then integrated in time using a third-order Runga–Kutta technique. The overall reaction scheme differs little from those used conventional excimer laser models.[9] Particularly important excitation mechanisms with respect to the Ar laser are discussed below.

TABLE I. Ar species in model. (Note: Ar^T represents higher excited states.)

Species	Energy (eV)
$Ar(4s)$	11.60
$Ar(4p)$	13.17
$Ar(4p')$	13.33
$Ar(3d)$	13.86
$Ar(3d')$	14.30
Ar^T	15.18
Ar^+	15.76
Ar_2^*	11.06
Ar_2^+	14.50

The proposed major kinetic pathways in our model are schematically shown in Fig. 2. It has previously been suggested that the Ar laser levels are populated by recombination of Ar^+ and Ar_2^+.[12] It has also been suggested that dissociative recombination of $HeAr^+$ is an important pumping mechanism for the upper laser level.[3,5,6] The competition between formation of Ar^+, Ar_2^+, and $HeAr^+$ may therefore largely determine the performance of the laser as a function of gas mixture. Recent experimental results have shown that dissociative recombination of Ar_2^+, primarily produces $Ar(4s)$ (branching ratio 0.9), with a small fraction producing the lower laser levels, $Ar(4p)$.[28] Therefore, population of the upper laser level must depend on dissociative recombination of Ar^+ or $HeAr^+$. Previous studies have suggested that collisional radiative recombination of Ar^+ followed by quenching from higher excited states of Ar is the primary pumping mechanism.[12] We found that when including a detailed accounting of the Ar excited-state kinetics that this mechanism did not reproduce experimental trends for the pumping conditions of interest. This point will be discussed further below.

TABLE II. Pertinent reactions in the He/Ar laser system.[a]

Reaction	W values (1 atm; He/Ar=99.7/0.3)	Ref.
	Electron beam excitation	
$e+He \rightarrow He^+ + e + e$	47.7 eV/event	b
$e+He \rightarrow He^{**} + e + e$	101.2 eV/event	b
$e+He \rightarrow He^{*} + e + e$	250.4 eV/event	b
$e+Ar \rightarrow Ar^+ + e + e$	767.3 eV/event	b
$e+Ar \rightarrow Ar^T + e + e$	534.8 eV/event	b
$e+Ar \rightarrow Ar(4p') + e + e$	534.8 eV/event	b
$e+Ar \rightarrow Ar(4p) + e + e$	534.8 eV/event	b
$e+Ar \rightarrow Ar(3d') + e + e$	534.8 eV/event	b
$e+Ar \rightarrow Ar(3d) + e + e$	534.8 eV/event	b
$e+Ar \rightarrow Ar(4s) + e + e$	2097.9 eV/event	b
Reaction	**Rate coefficient[c]**	**Ref.**
	Electron impact excitation and superelastic collisions	
$e+Ar \rightarrow Ar^+ + e$	$4.0\times10^{-12}T_e^{0.5}\exp(-15.8/T_e)$	16
$e+Ar \rightarrow Ar(3d,3d') + e$	$2.0\times10^{-12}T_e^{0.5}\exp(-14.3/T_e)$	16
$b(3d)=0.5$		
$b(3d')=0.5$		
$e+Ar \rightarrow Ar(4p,4p') + e$	$5.0\times10^{-12}T_e^{0.5}\exp(-13.3/T_e)$	16
$b(4p)=0.5$		
$b(4p')=0.5$		
$e+Ar \rightarrow Ar(4s) + e$	$1.0\times10^{-11}T_e^{0.75}\exp(-11.6/T_e)$	16
$e+He \rightarrow He^+ + e$	$1.5\times10^{-9}T_e^{0.68}\exp(-24.6/T_e)$	17
$e+He \rightarrow He^* + e$	$4.2\times10^{-9}T_e^{0.31}\exp(-19.8/T_e)$	17
$e+He \rightarrow He^{**} + e$	$7.7\times10^{-9}T_e^{0.31}\exp(-20.9/T_e)$	17
$e+He^* \rightarrow He^{**} + e$	$4.36\times10^{-7}T_e^{0.32}\exp(-1.14/T_e)$	17
$e+He^* \rightarrow He^+ + e + e$	$1.28\times10^{-7}T_e^{0.6}\exp(-4.78/T_e)$	17
$e+Ar^* \rightarrow Ar^+ + e + e$	$1.0\times10^{-10}T_e^{3}\exp(-4.16/T_e)$	16
$e+Ar^* \rightarrow Ar(3d,3d') + e$	$2.0\times10^{-7}T_e\exp(-2.7/T_e)$	16
$b(3d)=0.5$		
$b(3d')=0.5$		
$e+Ar^* \rightarrow Ar(4p,4p') + e$	$2.0\times10^{-7}T_e\exp(-13.3/T_e)$	16
$b(4p)=0.5$		
$b(4p')=0.5$		
	Dissociative recombination reaction	
$He_2^+ + e \rightarrow He^* + He$	$5\times10^{-9}T_e^{-0.5}$	18
$Ar_2^+ + e \rightarrow Ar(3d,3d') + Ar$	$4\times10^{-8}T_e^{-0.67}$	19
$b(3d)=0.75$		
$b(3d')=0.25$		
$Ar_2^+ + e \rightarrow Ar(4p,4p') + Ar$	$6\times10^{-8}T_e^{-0.67}$	19
$b(4p)=0.833$		
$b(4p')=0.167$		
$Ar_2^+ + e \rightarrow Ar(4s) + Ar$	$6\times10^{-7}T_e^{-0.67}$	19
$HeAr^+ + e \rightarrow Ar(3d,3d') + e$	$6.3\times10^{-8}T_e^{-0.5}$	d
$b(3d)=0.71$		
$b(3d')=0.29$		
$HeAr^+ + e \rightarrow Ar(4p,4p') + He$	$7\times10^{-10}T_e^{-0.5}$	d
$b(4p)=0.5$		
$b(4p')=0.5$		
	Three-body association	
$He^+ + He + He \rightarrow He_2^+ + He$	$2\times10^{-31}\ cm^6\ s^{-1}$	20
$Ar^+ + Ar + Ar \rightarrow Ar_2^+ + Ar$	$2.5\times10^{-31}\ cm^6\ s^{-1}$	21
$He^+ + He + Ar \rightarrow HeAr^+ + He$	$2.5\times10^{-32}\ cm^6\ s^{-1}$	d
$He^+ + Ar + Ar \rightarrow Ar_2^+ + He$	$1.0\times10^{-31}\ cm^6\ s^{-1}$	d
	Penning ionization and charge and excitation transfer	
$He_2^+ + Ar \rightarrow Ar^+ + He + He$	2.2×10^{-10}	22
$He_2^+ + Ar + M \rightarrow Ar^+ + He + He + M$	$2.4\times10^{-29}\ cm^6\ s^{-1}$	22
$Ar(4s) + Ar(4s) \rightarrow Ar^+ + Ar + e$	5.0×10^{-10}	23
$Ar(4p,4p') + Ar(4p,4p') \rightarrow Ar^+ + Ar + e$	5.0×10^{-10}	23
$He^* + He^* \rightarrow He^+ + He + e$	2.7×10^{-10}	17
$He_2^* + Ar \rightarrow Ar^+ + e + He + He$	3.1×10^{-10}	18

TABLE II. (*Continued.*)

Reaction	Rate coefficient[c]	Ref.
	Heavy particle quenching	
$Ar^{**}+Ar \rightarrow Ar(3d,3d')+Ar$	1.0×10^{-11}	24
$Ar(3d,3d')+Ar \rightarrow Ar(4p,4p')+Ar$	1.0×10^{-11}	24
$Ar(4p,4p') \rightarrow Ar(4s)$	1.0×10^{-10}	24
	Collisional radiative recombination	
$Ar^{+}+e+e \rightarrow Ar^{**}+e$	$7.2\times10^{-27}T_e^{-4.5}$ cm^6 s^{-1}	25
$Ar^{+}+e+M \rightarrow Ar^{**}+M$	$9.3\times10^{-23}T_e^{-2.5}$ cm^6 s^{-1}	25
$He^{+}+e+e \rightarrow He^{**}+e$	$5.1\times10^{-27}T_e^{-4.5}$ cm^6 s^{-1}	26
$He^{+}+e+M \rightarrow He^{**}+M$	$9.3\times10^{-23}T_e^{-2.5}$ cm^6 s^{-1}	25
	Radiative relaxation	
$Ar^{**} \rightarrow Ar(3d,3d')$	6.2×10^{7} s^{-1}	24
$Ar(3d,3d') \rightarrow Ar(4p,4p')$	9.5×10^{6} s^{-1}	24
$Ar(4p,4p') \rightarrow Ar(4s)$	7.0×10^{7} s^{-1}	24
	Line broadening collisions	
$Ar(3d)+He \rightarrow Ar(3d)+He$	7.0×10^{-10}	10
$Ar(3d')+He \rightarrow Ar3d')+He$	7.0×10^{-10}	10
$Ar(3d)+Ar \rightarrow Ar(3d)+Ar$	9.0×10^{-8}	10
$Ar(3d')+Ar \rightarrow Ar(3d')+Ar$	9.0×10^{-8}	10

[a]A complete listing of reactions can be found in Ref. 14 or requested from the authors.
[b]Computed by Monte Carlo model described in Ref. 15.
[c]Rate coefficients have units of cm^3 s^{-1} unless noted otherwise. $b(3d)$ denotes branching ratio to $3d$. T_e is the electron temperature in eV.
[d]Estimated. See text.

The fact that recombination of neither Ar^+ or Ar_2^+ as a precursor of the upper laser level allowed us to reproduce experiments motivated us to examine the contributions of dissociative recombination of $HeAr^+$ to pumping the upper laser level. The rate coefficients for the formation and dissociative recombination of He_2^+ and Ar_2^+, as well as charge transfer reactions between He^+, He_2^+, Ar^+, and Ar_2^+ are fairly well known.[18,29,30] Unfortunately, little is known about the formation and recombination of $HeAr^+$. We derived values for these rate coefficients by parametrizing the model and comparing our predictions for laser power to experiments. Although this exercise does not produce a unique set of rate coefficients, it does provide a self-consistent reaction mechanism which reproduces experimental behavior, and therefore is useful for scaling studies.

In deriving these rate coefficients, we relied on a few simple arguments to begin with. For example, the formation of $HeAr^+$ by $Ar^+ + He + Ar \rightarrow HeAr^+ + Ar$ should be smaller than the rate of formation of Ar_2^+ by $Ar^+ + Ar + Ar \rightarrow Ar_2^+$ (rate coefficient 2.5×10^{-31} cm^6 s^{-1}). This requirement stems from the necessity to account for the experimentally observed reduction in laser power at high Ar mole fraction. [At high mole fractions of Ar, contributions of dissociative recombination of Ar_2^+ to $Ar(4p)$ quenches laser oscillation.] Analogously, the rate coefficient for formation of $HeAr^+$ by $Ar^+ + He + He \rightarrow HeAr^+ + He$ should be smaller than the analogous reaction with Ar as the stabilizing collision partner to account for the fact that laser oscillation is weak at small mole fractions of Ar (<0.001). Following these arguments with extensive parametric studies, we derived rate coefficients of 2.5×10^{-32} cm^6 s^{-1} for $Ar^+ + He + Ar \rightarrow HeAr^+ + Ar$; and 1.0×10^{-32} cm^6 s^{-1} for $Ar^+ + He + He \rightarrow HeAr^+ + He$.

Due to the lower binding energy of $HeAr^+$ compared to Ar_2^+, its dissociative recombination should populate states higher in the Ar manifold than Ar_2^+. After parametric studies, we assigned a branching of 0.01 to $Ar(4d)$ and 0.99 to $Ar(3d')$ for dissociative recombination of $HeAr^+$. The results of model also suggest that the rate coefficient for dissociative recombination of $HeAr^+$ should be smaller than that of Ar_2^+ ($7.0\times10^{-7}T_e^{-0.5}$ cm^3 s^{-1}) and a value of ($7.0\times10^{-8}T_e^{-0.5}$ cm^3 s^{-1}) was assigned.

The dominant clearing mechanisms for lower laser levels are radiative relaxation to $Ar(4s)$ and collisional quenching by heavy particles. The collisions either remove $Ar(4p)$ by forming argon dimers or quench the lower laser levels to $Ar(4s)$. The argon metastables are then dominantly removed by formation of Ar dimers, are elevated by electron impact to higher excited states or are ionized by electron impact. Under typical low-power deposition conditions (He/Ar=99.7/0.03), 48% of $Ar(4s)$ atoms are removed by forming Ar dimers, 20% are excited to higher lying levels and less than 1% are ionized by electron impact collisions. The latter two processes contribute to the electronization cycle which allows laser efficiencies to approach the quantum efficiency based on excitation from the ground state. The electroionization cycle of the Ar laser is not as efficient as in the Xe laser at low pump rates (<100 s W/cm^3) due to the relatively large energy separation between the metastable states and higher excited and ionic

states in Ar compared to Xe. This issue will be discussed further in the next section.

Effects of gas heating were neglected in the model with the temperature being fixed at 300 K. Gas heating has been shown to be an important consideration in the Xe atomic laser where increasing gas temperature leads to higher levels of electron collision mixing of the laser levels and eventual quenching of the inversion.[7,10] By ignoring gas heating in this model, our predictions for laser performance at high-energy loading are best case analyses.

The results of our model have been compared to experiments performed by Hebner and Hays for fission-fragment excitation of the Ar laser.[1,2] The experiments were performed using the Sandia National Laboratory SPR-III fast burst reactor as a source of fast neutrons. The laser cell gain region was 60 cm long with a rectangular cross section of 1×7 cm^2. The laser cavity was formed by a 4 m radius of curvature (5 cm diameter) maximum reflectivity dielectric mirror, and a flat dielectric output couplers (5 cm diameter) having various reflectivities. The laser output was detected through a bandpass filter with an InAs photodiode. The laser cell was lined with enriched uranium oxide foils. The fast fission neutrons from the reactor were moderated to thermal energies by high-density polyethylene surrounding the laser cell. The moderated neutrons induced fissions in the foils, producing energetic fission fragments. A fraction of the fission fragments exit the coatings and deposit their kinetic energy in the gas as ionization and excitation.

III. PARAMETRIC STUDY OF THE PERFORMANCE OF THE ARGON LASER

Laser parameters as a function of Ar mole fraction in He/Ar mixtures were investigated using the experimental conditions of Hebner and Hays.[1,2] The gas pressure was 760 Torr and the quasicontinuous power deposition was 100 W cm^{-3}. Predictions for electron temperature and electron density are shown in Fig. 3(a) for Ar mole fractions of 10^{-3} to 10%. Ion densities are shown in Fig. 3(b). The electron density decreases with increasing Ar mole fraction. This is somewhat counter-intuitive since the W value for ionization decreases (more efficient ionization) as the He mole fraction decreases. However, at low Ar mole fractions, the predominant ions are He^+ and He_2^+. He_2^+ has a small rate coefficient for dissociative recombination ($5.0\times10^{-9}T_e^{-0.5}$ cm^3 s^{-1}) compared to Ar_2^+ and so the electron density is large, because the rate of loss is small. As the Ar mole fraction increases, $HeAr^+$ and Ar_2^+ are larger proportions of the ion population. Even though the direct formation of Ar ions is small, Ar^+ are produced by charge exchange from He_2^+ and Penning ionizations from He* and He_2^*. Following formation of Ar^+, $HeAr^+$ is formed by three body association reactions. The $HeAr^+$ ion has a maximum density at an Ar mole fraction of $\simeq0.1\%$ whereas the Ar_2^+ density monotonically increases over the cited range of Ar mole fraction due to the more efficient three body association rate.

The electron temperature decreases with increasing Ar mole fraction (0.6–0.35 eV) due primarily to increasing

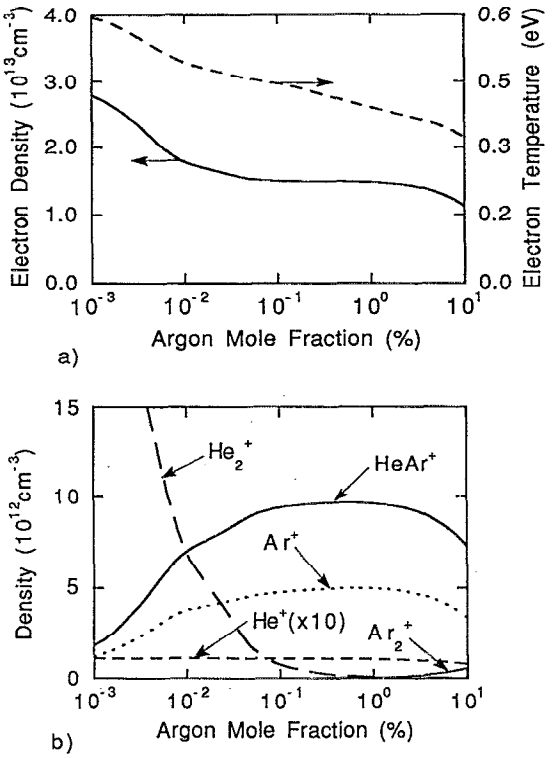

FIG. 3. Plasma parameters as a function of Ar mole fraction in He/Ar mixtures (total pressure 760 Torr). (a) Electron temperature and density and (b) ion densities. The power deposition is 100 W cm^{-3}. As the Ar mole fraction increases, electron temperature and electron density decrease. At intermediate Ar mole fractions $HeAr^+$ is the dominant ion which, by dissociative recombination, excites the upper laser level. Competition from formation of Ar_2^+ decreases the density of $HeAr^+$ at high Ar mole fractions.

rate of momentum transfer resulting from collisions with Ar and its excited states. An important difference between our results and those of Wilson *et al.*[12] relate to the electron temperature. Wilson *et al.* assumed that the electron temperature is near ambient (300 K). The electron temperature in our model is larger due to a recombination heating effect. Since the cross section for recombination scales as $1/\epsilon^n$ (ϵ is the electron energy, $n=0.5$–1.5), the lowest-energy electrons are removed by recombination at the highest rates. This results in raising the average electron energy. Due to Wilson *et al.* using a low electron temperature, their results emphasized collisional radiative recombination of Ar^+, which scales as $T_e^{-4.5}$, as a precursor to the upper laser level. In our model, which produces a higher T_e, collisional radiative recombination does not significantly affect the kinetics.

Predicted and experimental laser power efficiency for oscillation at 1.79 μm are shown in Fig. 4 as a function of Ar mole fraction. The maximum laser power efficiency occurs at an Ar mole fraction of $\simeq1\%$. Laser oscillation is quenched at Ar mole fractions exceeding 10%. Our predictions agree well with the experiments at Ar mole fractions at and above the peak efficiency, but diverge somewhat at lower mole fractions. The dependence of laser

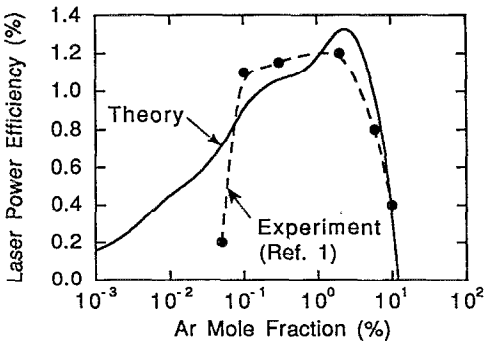

FIG. 4. Calculated and experimental laser power efficiency at 1.79 μm as a function of Ar mole fraction for a power deposition of 100 W cm^{-3} and a total pressure of 760 Torr. The decrease in laser power at high Ar mole fraction results from a competition between formation of Ar_2^+ and $HeAr^+$.

power efficiency on Ar mole fraction can be explained by the ion densities shown in Fig. 3(b).

At low Ar mole fractions, the dominant ions are He^+ and He_2^+ which do not directly contribute to exciting the upper laser levels. As the Ar mole fraction increases towards the optimum values, the densities of $HeAr^+$ and Ar^+ increase due to the more rapid charge transfer to Ar from He^+ and He_2^+, and more power directly dissipated by ionization of Ar. In our reaction scheme, the upper laser level is dominantly excited by dissociative recombination of $HeAr^+$. Although the rate coefficient for the dissociative recombination of $HeAr^+$ is not large, the large electron and $HeAr^+$ densities sustain the high rate of recombination to the upper laser level. The increase in Ar_2^+ at higher Ar mole fractions of argon competes with the formation of $HeAr^+$, thereby decreasing the density of $HeAr^+$. Only 10% of Ar_2^+ recombines to form the lower laser level. Therefore the decrease in laser power at high Ar mole fractions is largely a result of a decrease in the rate of pumping of the upper laser level due to the decrease in the density of $HeAr^+$ rather than a large increase in the rate of pumping of the lower laser level.

The density of Ar^+ scales similarly to that of $HeAr^+$ with Ar mole fraction and so could be identified as a dominant precursor to the upper laser level. The rate coefficient for collisional radiative recombination of Ar^+ scales as $T_e^{-4.5}$. Therefore at our moderate electron temperatures, its rate of recombination is small. Ar^+ is dominantly lost by dimer forming reactions rather than by recombination. Lower plasma densities or other conditions which result in lower electron temperatures, as in the work of Wilson *et al.*,[12] will significantly increase the contribution of collisional radiative recombination of Ar^+ to pumping the upper laser level.

The electron temperature and density as a function of pressure are shown in Fig. 5(a). The Ar mole fraction is constant at 0.3%. As the pressure increases, the electron temperature decreases due to the larger rate of momentum transfer. The electron density decreases with increasing pressure due to the lower electron temperature which results in larger rates of dissociative recombination. The higher pressure also produces larger rates of three body dimer ion forming collisions which are followed by dissociative recombination. The density of ions as a function of pressure are shown in Fig. 5(b). The densities of He^+ and Ar^+ decrease with increasing pressure due to the increasing rate of three-body association reactions which form He_2^+, $HeAr^+$, and Ar_2^+. As the pressure increases further,

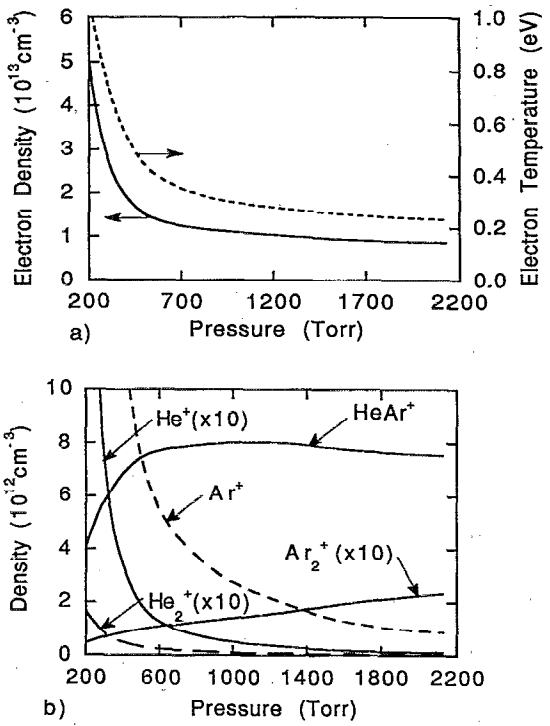

FIG. 5. Plasma parameters as a function of pressure in He/Ar=99.7/0.3 mixtures. (a) Electron temperature and density and (b) ion densities. The power deposition is 75 W cm^{-3}. The electron temperature decreases with increasing pressure due to more rapid rates of thermalization. Increasing pressure results in more rapid formation of dimer ions. The electron density then decreases due to high rates of dissociative recombination.

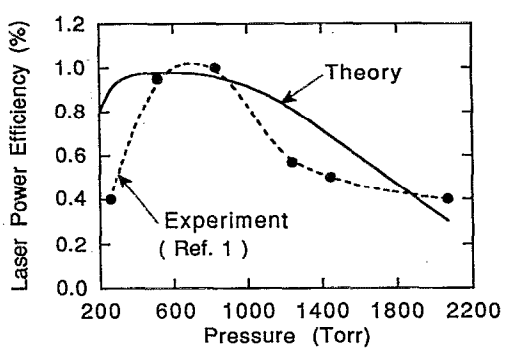

FIG. 6. Calculated and experimental laser power efficiency at 1.79 μm as a function of pressure. (The Ar mole fraction is 0.3%.) The power deposition is 75 W cm^3. Laser power efficiency decreases at high He pressure due to collisional broadening and reduction in the density of $HeAr^+$.

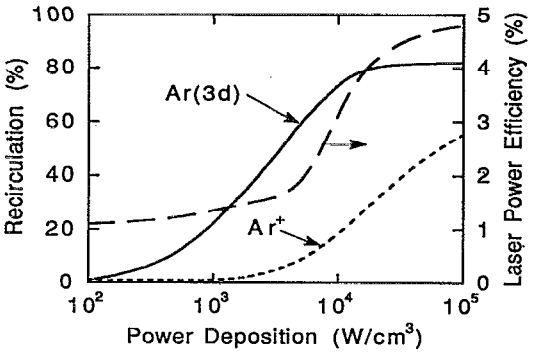

FIG. 7. Fraction of rates of formation of Ar^+ and Ar(3*d*) attributed to recirculation from the Ar metastables as a function of power. Electroionization increases sharply at pump rates above 10 kW/cm^3. Predicted laser power efficiency is also shown (in the absence of gas heating).

the enhanced dissociative recombination rates brought by the lower electron temperature limits the further increase of the dimer ions.

Calculated and experimental laser power efficiency as a function of helium pressure are shown in Fig. 6 for the 1.79 μm transition. The experimental results show that the laser power efficiency optimizes near a pressure of 700–800 Torr. The initial rise of the efficiency is due to the increase of the formation of the precursor $HeAr^+$. At high pressures, the formation of Ar_2^+ competes with the formation of $HeAr^+$ and so decreases the rate of pumping of the upper laser level. As the pressure increases, collisional broadening of the laser levels also increases, thereby decreasing gain. Additional quenching of the laser levels by dimer formation at the higher pressure also contribute to lowering gain. The predicted laser power efficiencies as a function of pressure generally reproduce the experimental trends; however we predict higher laser efficiencies at low gas pressures.

The power efficiency of the Ar laser generally increases with increasing power deposition. For example, in the absence of significant gas heating at a power deposition of 100 W cm^{-3}. Hebner and Hays[1,2] obtained a maximum laser power efficiency of 1.4%. Dudin *et al.*[5] obtained 2.8% laser power efficiency at 10 kW cm^{-3}. Our predictions for laser power efficiencies are shown in Fig. 7 without gas heating. The increasing power efficiency may be attributable to increasing contributions of electroionization at the higher-power levels. Since both the Ar(4*s*) and electron densities scale with power *P*, the contributions of electroionization to populating the upper laser level should scale as P^2, whereas "direct" excitation scales as *P*. We previously noted that for the experiments of Hebner and Hays,[1,2] the contributions of electroionization are small. However, the high electron densities and high metastable densities obtained at moderate pump rates allow an efficient electroionization cycle. This is also demonstrated in Fig. 7 where we have plotted the fraction of the formation rates of Ar(3*d*) and Ar^+ which are attributable to recirculation as a function of pump rates. The recirculation

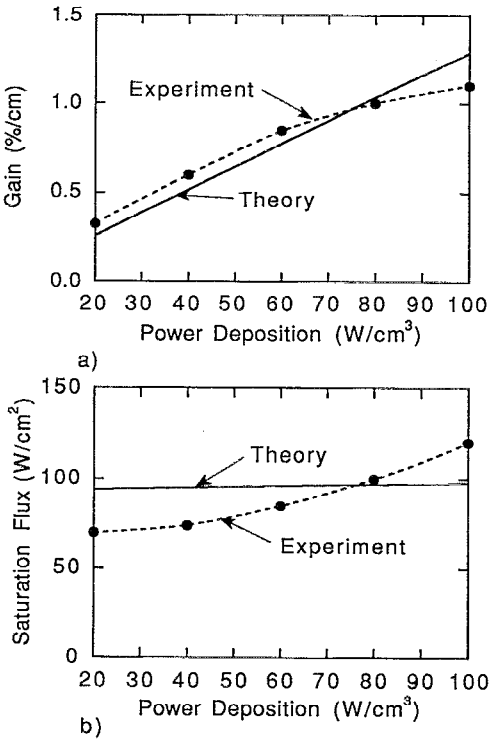

FIG. 8. Calculated and experimental laser parameters (1.79 μm) as a function of power deposition; (a) gain and (b) saturation flux. The gas mixture is He/Ar=99.7/0.3 at 760 Torr. Gain increases nearly linearly with power deposition with some amount of saturation at high powers, possibly a consequence of gas heating.

increases with increasing power deposition thereby allowing more efficient laser operation.

Calculated gain and saturation flux of the Ar laser are compared to the experiments[1,2] in Fig. 8 as a function of power deposition for the 1.79 μm transition. The gain linearly increases with increasing power deposition at low powers. Experimentally, the gain begins to slightly saturate at higher power deposition, whereas the calculations continue to predict a linear dependence on power deposition. This discrepancy may be attributed to gas heating effects which are not included in this model. (In Xe atomic lasers, it is known that gas heating leads to increased electron collision quenching of the laser levels and a decrease in gain.[10]) The experimentally derived saturation flux increases with increasing power deposition whereas the calculated values are relatively constant. The increase in the saturation intensity may again be attributable to gas heating effects which increase the electron collision quenching of the laser levels.

IV. CONCLUDING REMARKS

The kinetics of the high-pressure atomic Ar laser using He/Ar gas mixtures have been theoretically investigated and the results have been compared to experiments using fission fragment excitation. A reaction mechanism in which dissociative recombination of $HeAr^+$ is a major precursor to the upper laser level reproduces experiment mea-

surements of laser power efficiency as a function of Ar mole fraction and He pressure. For our conditions, collisional radiative recombination of Ar^+ is insufficient to account for the observed gain due to a greater than thermal electron temperature which decreases its rate. At high Ar mole fractions, formation of Ar_2^+ competes with formation of $HeAr^+$, thereby decreasing the excitation of the upper laser level and quenching laser oscillation at high Ar mole fractions. Contributions of dissociative recombination of Ar_2^+ to the lower laser level, though small, also contribute to the quenching.

ACKNOWLEDGMENTS

The authors wish to express their thanks to G. Hebner and G. Hays for valuable advice on Ar laser kinetics, and access to their experimental results prior to publication. This work was supported by Sandia National Laboratory and by the National Science Foundation (ECS-91-09362 and CTS-91-13215).

[1] G. A. Hebner and G. N. Hays, J. Appl. Phys. **71**, 1610 (1992).
[2] G. A. Hebner and G. N. Hays, IEEE J. Quantum Electron. **29**, 2356 (1993).
[3] A. M. Voinov, V. N. Krivonosov, S. P. Mel'nikov, I. N. Mochkaev, and A. A. Sinyanskii, Sov. J. Quantum Electron. **21**, 157 (1991).
[4] S. P. Mel'nikov and A. A. Sinyanskii, Sov. J. Quantum Electron. **21**, 1332 (1991).
[5] A. Yu. Dudin, D. A. Zayarnyi, L. V. Semenova, N. N. Ustinovskii, I. V. Kholin, and A. Yu. Chugunov, Sov. J. Quantum Electron. **21**, 833 (1991).
[6] B. M. Berkeliev, V. A. Dolgikh, I. G. Rudoi, and A. M. Sorka, Sov. J. Quantum Electron, **21**, 250 (1991).
[7] G. A. Hebner, J. W. Shon, and M. J. Kushner, Appl. Phys. Lett. **63**, 2872 (1993).
[8] S. A. Lawton, J. B. Richards, L. A. Newman, L. Specht, and T. A. DeTemple, J. Appl. Phys. **50**, 3888 (1979).
[9] F. Kannari, W. D. Kimura, and J. J. Ewing, J. Appl. Phys. **66**, 5131 (1989).
[10] J. W. Shon, M. J. Kushner, G. A. Hebner, and G. N. Hays, J. Appl. Phys. **73**, 2686 (1993).
[11] J. W. Shon, R. L. Rhoads, J. T. Verdeyen, and M. J. Kushner, J. Appl. Phys. **73**, 8059 (1993).
[12] J. W. Wilson, R. J. DeYoung, and W. L. Harries, J. Appl. Phys. **50**, 1226 (1979).
[13] G. Basov, A. Yu Chugunov, V. A. Danilychev, I. V. Kholin, and M. N. Ustinovskii, IEEE J. Quantum Electron. **QE-19**, 126 (1983).
[14] J. W. Shon, Ph.D. thesis, University of Illinois at Urbana (1993).
[15] M. J. Kushner, J. Appl. Phys. **66**, 2297 (1989).
[16] F. Kannari, A. Suda, M. Obara, and T. Fujioka, IEEE J. Quantum Electron. **QE-19**, 1587 (1983).
[17] R. Deloche, P. Monchicourt, M. Cheret, and F. Lambert, Phys. Rev. A **13**, 1140 (1976).
[18] C. B. Collins and F. W. Lee, J. Chem. Phys. **68**, 1391 (1978).
[19] Y. J. Shiu and M. A. Biondi, Phys. Rev. A **17**, 868 (1978).
[20] D. Smith and M. J. Copsey, J. Phys. B **1**, 650 (1968).
[21] D. Smith and P. R. Cromey, J. Phys. B **1**, 638 (1968).
[22] C. B. Collins and F. W. Lee, J. Chem. Phys. **68**, 1391 (1978).
[23] P. K. Leichner and R. J. Ericson, Phys. Rev. A **9**, 251 (1974).
[24] R. S. F. Chang and D. W. Setser, J. Chem. Phys. **69**, 3885 (1978).
[25] M. Biondi, in *Principles of Laser Plasmas*, edited by G. Bekefi (Wiley–Interscience, New York, 1976), Chap. 4.
[26] C. B. Collins, H. S. Hicks, W. E. Wells, and R. Burton, Phys. Rev. A **6**, 1545 (1972).
[27] T. J. Moratz, T. D. Saunders, and M. J. Kushner, J. Appl. Phys. **64**, 3799 (1988).
[28] J. R. Peterson, 44th Gaseous Electronics Conference, Albuquerque, NM. October, 1991, Paper MC-16.
[29] J. Bretagne, J. Godart, and V. Puech, Beitr. Plasmaphys. **23**, 295 (1983).
[30] C. B. Collins and F. W. Lee, J. Chem. Phys. **70**, 1275 (1979).